An investigation of chaotic Kolmogorov flows

N. Platt and L. Sirovich
Center for Fluid Mechanics and Division of Applied Mathematics, Brown University, Providence, Rhode Island 02912

N. Fitzmaurice
Department of Mathematics, Case Western Reserve University, Cleveland, Ohio 44106

(Received 28 November 1988; accepted 14 December 1990)

A two-dimensional flow governed by the incompressible Navier–Stokes equations with a steady spatially periodic forcing (known as the Kolmogorov flow) is numerically simulated. The behavior of the flow and its transition states as the Reynolds number Re varies is investigated in detail, as well as a number of the flow features. A sequence of bifurcations is shown to take place in the flow as Re varied. Two main regimes of the flow have been observed: small and large scale structure regimes corresponding to different ranges of Re. Each of the regimes includes a number of periodic, chaotic, and relaminarization windows. In addition, each range contains a chaotic window with nonunique chaotic attractors. Spatially disordered, but temporally steady states have been discovered in the large scale structure regime. Features of the diverse cases are displayed in terms of the temporal power spectrum, Poincaré sections and, where possible, Lyapunov exponents and Lyapunov dimension.

I. INTRODUCTION

It is now well established that a number of dissipative chaotic fluid flows may require relatively few dimensions for their long-term dynamical description.[1-4] This has been examined perhaps in greatest detail for fluid models such as the Ginzburg–Landau (G–L) equation,[5-8] an equation which results from the study of the critical point in a variety of stability problems.[9-12] For closed fluid systems such as Rayleigh–Bénard (R–B) convection and Taylor–Couette flow there is abundant evidence that the early stages of chaos are low dimensional. For R–B convection there also exists a numerical simulation that details the variation of dimension with Rayleigh number.[13]

In this paper we consider a simple fluid flow that exhibits chaotic behavior and that is amenable to detailed examination. This flow, governed by the incompressible Navier–Stokes equations, is generated and maintained by a spatially periodic time-independent forcing of the fluid. It is sometimes referred to as the Kolmogorov flow (Arnold and Meshalkin[14]). This flow was originally introduced by Kolmogorov in a seminar as an example of a simple linear stability problem. The stability of the primary flow has been reported on by Meshalkin and Sinai[15] and by Green.[16] The flow is known to become linearly unstable at a critical Reynolds number, Re_c, of $\sqrt{2}$[15,16] (the Reynolds number is defined in the following section), beyond which a stationary cellular pattern appears.[17] At sufficiently high Re the cellular pattern itself becomes unstable and the resulting flow is unsteady and chaotic. Kraichnan[18] and Batchelor[19] have shown that at sufficiently high Re two-dimensional turbulent flow exhibit an energy cascade toward low wave numbers (the infamous reverse cascade) and an entropy cascade toward high wave numbers. This cascade process appears to be in effect in our calculations even though the Re number is relatively low. An alternate view of this effect, in the present instance, is that the flow is unstable to long wavelength disturbances. The general instability of short wavelength structures to long wavelength disturbances has been investigated by Yakhot and Sivashinsky, and under sufficiently anisotropic conditions, their study lead to the notion of negative viscosity for the long wavelengths,[20,21] since the growth rate is proportional to the square of the wave number.

Our investigation is, in large part, numerical in nature. We examine in some detail the behavior of the flow and its transition states for a range of the bifurcation parameter Re. We use Poincaré sections to examine the chaotic attractor of the flow, and apply the Kaplan–Yorke formula[22] to calculate the dimension of the chaotic attractor when it is possible. A number of remarkable features of the flow were discovered. These include windows of relaminarization in the parameter space; attractors which are *nonunique* in the sense that only some part of the attractor can be visited; and spatially disordered but temporally steady states.

We will be careful throughout this paper to use the term *chaotic* instead of the term *turbulent.* In particular we are referring to flows that when looked at in the time domain have broadband energy spectra. These flows also exhibit sensitive dependence on initial data (they have positive Lyapunov exponents). Thus by generally accepted criteria the flows are temporally chaotic. However, as will be seen, relatively few spatial Fourier modes are active and the broadbanded spatial spectrum characteristic of the true turbulence is not seen. Nevertheless, the flow is chaotic in its Eulerian description and should not be confused with *Lagrangian turbulence*[23-25] in which the velocity fields are to a high degree laminar.

Recently we became aware of the investigation of the Kolmogorov flow by She.[26,27] While there is some unavoidable overlap, the two investigations are largely complimen-

 0899-8213/91/040681-16$02.00

tary. She's work is also mainly numerical and concentrates on the high end of the Re range. (A minor difference is that he uses a higher value for the frequency of the forcing function.) The mathematical tools used also differ. We will make extensive use of the power spectra, Poincaré sections, Lyapunov spectra, and flow visualizations for the investigation, while She relies mainly on time series and phase portraits. Several issues are viewed differently by us and we comment on these in the text. She's further work done in collaboration with Nicolaenko is concentrated on the symmetry breaking homoclinic chaos[28,29] occurring beyond the Re range covered in this study.

II. KOLMOGOROV FLOW

We consider the forced incompressible Navier–Stokes equations in two dimensions,

$$\partial'_x u' + \partial'_y v' = \nabla\cdot\mathbf{u}' = 0, \tag{1}$$

$$\frac{d}{dt'}\mathbf{u}' + \frac{\nabla p'}{\rho} = \nu\nabla'^2\mathbf{u}' + \chi \sin ky'\mathbf{e}_x. \tag{2}$$

In preparation for the normalization given below, dimensional quantities are denoted by primes and $\mathbf{e}_x$ denotes the unit vector in the x direction. This system has the solution or *fixed point*,

$$\mathbf{u}' = \mathbf{U}' = [\chi\mathbf{e}_x/(k^2\nu)]\sin ky'. \tag{3}$$

A Reynolds number for the flow may be naturally based on the maximum speed of this field, $\chi/\nu k^2$ and the length scale k^{-1}, thus

$$\mathrm{Re} = \chi/(k^3\nu^2). \tag{4}$$

(A Reynolds number could also be based on the wavelength and maximum speed giving value of 2π Re in terms of our parameter.)

The linear stability of (3) can be analyzed by writing

$$\mathbf{u}' = \mathbf{U}' + \delta\mathbf{u}'(y)\exp(ikx + \sigma t) \tag{5}$$

and investigating the resulting Orr–Sommerfeld equation.[30] It is found that instability first sets in at[15,16]

$$\mathrm{Re} = \mathrm{Re}_c = \sqrt{2} \tag{6}$$

and is due to disturbances of infinitely long wavelength. Moreover, it can be shown that disturbances with $\alpha k > 1$ never destabilize $\mathbf{U}'$.

Thus, according to the stability analysis, the domain must be large in some sense in order for us to include growing modes. For computational purposes we fix the domain size and regard the spatial forcing frequency as the bifurcation parameter. With this in mind we choose the following normalization:

$$\mathbf{u} = \frac{\nu k^2\mathbf{u}'}{\chi}, \quad \mathbf{x} = \frac{k\mathbf{x}'}{n}, \quad t = \frac{\chi t'}{(nk\nu)}, \quad p = \frac{p'\nu^2k^4}{\chi^2}, \tag{7}$$

where n is an integer that specifies the spatial frequency of the forcing. Under this normalization the Navier–Stokes equations become

$$\nabla\cdot\mathbf{u} = 0, \tag{8}$$

$$\frac{d\mathbf{u}}{dt} + \nabla p = \frac{1}{\Omega}\nabla^2\mathbf{u} + \frac{n^2}{\Omega}\mathbf{e}_x \sin ny \tag{9}$$

with periodic boundary conditions in two directions

$$0 \leqslant x, \quad y \leqslant 2\pi. \tag{10}$$

Here

$$\Omega = n\chi/(\nu^2k^3) = n\,\mathrm{Re} \tag{11}$$

is the bifurcation parameter. In this format the critical value of Ω is

$$\Omega_c = n\,\mathrm{Re}_c = n\sqrt{2}. \tag{12}$$

We will refer to the solutions of these equations as Kolmogorov flows.

Equations (8)–(10) are invariant under groups of transformation that we now discuss.[31] There are in fact two groups, one discrete and the other continuous.

Referring back to the notation of (9), n refers to the number of vertical cycles in the horizontal forcing. If $[u(x,y,t),v(x,y,t)] = \mathbf{u}$ is a solution then

$$g^k\mathbf{u} \equiv \left[(-1)^k u\left((-1)^k x, y + k\frac{\pi}{n}\right), v\left((-1)^k x, y + k\frac{\pi}{n}\right)\right], \quad k = 0,\ldots,2n-1, \tag{13}$$

are also (independent) solutions of the problem, i.e., they satisfy the equations and conditions of the problem. The generator of this cyclic group, g, is a *glide reflection*[32] of half-wavelength. In addition rotation through π is another group generator, i.e., if $\mathbf{u}$ is a Kolmogorov flow then

$$R\mathbf{u} \equiv [-u(-x,-y), -v(-x,-y)] \tag{14}$$

is one also. In all there are $4n$ elements in the discrete symmetry group for the Kolmogorov flow. Thus we might possibly obtain $4n$ distinct solutions to (8)–(10) from any one Kolmogorov flow. However, some of these may be redundant and the actual number of distinct solutions produced by the discrete symmetry group depends upon the number of symmetries the original solution trajectory possesses.

The remaining symmetry group is the group of translations in the x directions, i.e., if $\mathbf{u}$ is a solution then

$$T_l\mathbf{u} = [u(x+l,y), v(x+l,y)] \tag{15}$$

are also solutions to the problem for all $0 \leqslant l \leqslant 2\pi$.

III. COMPUTATIONAL METHOD

Based on the normalization given in the previous section we consider the computational domain

$$0 \leqslant x, \quad y \leqslant 2\pi \tag{16}$$

with periodic boundary conditions in the two directions (so the flow lies on the torus).

The natural method of choice for the investigation of (8)–(10) under the 2π-periodic boundary conditions is the pseudospectral method using Fourier expansions.[33] All derivatives are evaluated in the spectral space and updates are performed on the expansion coefficients of $\mathbf{u}(\mathbf{x},t)$. On the other hand, the nonlinear terms are evaluated in the physical space and then transformed back to the spectral space. The needed transformations are all efficiently done by the means of the fast Fourier transforms.

In a variation on the usual formulation we have used the following vector expansion set for our velocity field:

$$\mathbf{B}_{\mathbf{m}}(\mathbf{x}) = [(m_2, -m_1)/|\mathbf{m}|]\exp(i\mathbf{m}\cdot\mathbf{x}), \tag{17}$$

where $\mathbf{m}$ is the integer wave-number pair (m_1,m_2). Using such a basis we can expand $\mathbf{u}$ as

$$\mathbf{u}(\mathbf{x},t) = \sum_{\mathbf{m}} u_{\mathbf{m}}(t)\mathbf{B}_{\mathbf{m}}(\mathbf{x}), \tag{18}$$

where the sum is performed over all the components of the wave vector $\mathbf{m}$.

The basis elements are easily seen to be divergence free,

$$\nabla\cdot\mathbf{B}_{\mathbf{m}} = 0 \tag{19}$$

and complete in the space of square integrable 2π-periodic divergence-free vector functions. An advantage of this formulation is that because gradients of scalar functions (such as the pressure term in the Navier–Stokes equations) are orthogonal to the space of divergence-free functions,[34] these terms are eliminated entirely in a Galerkin formulation. A computational method of this type was first used by Leonard and Wray[35] in their study of the stability of pipe flows.

Throughout our study the underlying forcing frequency was taken to be $n = 4$ and so that the critical value of the bifurcation parameter Ω is

$$\Omega_c = 4\sqrt{2}. \tag{20}$$

We shall be interested in the long-term, asymptotic behavior of the flows developing from the primary flow

$$\mathbf{u} = \mathbf{U} = (\sin 4y/\Omega)\mathbf{e}_x, \tag{21}$$

which is a fixed point solution of (8)–(10). It was found that integrations based on initial data having particular symmetries gave rise to long-term solutions having the same symmetries (this serves as a test of the numerical code). Our interest was in more general solutions, so we used initial conditions that added small perturbations to all wave numbers of the primary flow. In particular, we set

$$\mathbf{u}_0 = \frac{1}{\Omega}\sin(4y)\mathbf{e}_x + \frac{10^{-4}}{2\Omega} \times \sum_{\substack{m_1>0 \\ m_2>0}} [(1+i)\mathbf{B}_{\mathbf{m}}(\mathbf{x}) - (1-i)\mathbf{B}_{-\mathbf{m}}(\mathbf{x})]. \tag{22}$$

If we write

$$\mathbf{u}_0 = (u_0, v_0) \tag{23}$$

then, for example, u_0 has the form

$$u_0 = \frac{1}{\Omega}\left(\sin 4y + 10^{-4}\sum_{\substack{m_1>0 \\ m_2>0}} \frac{m_2}{|\mathbf{m}|}[\cos(m_1x + m_2y) - \sin(m_1x + m_2y)]\right). \tag{24}$$

The computations were performed for the range

$$\Omega/\Omega_c \leqslant 12.5. \tag{25}$$

Several time-steppers were implemented in the code. For the purpose of computing Lyapunov exponents, which is discussed later, it was found that the self-starting Runge–Kutta schemes were the most convenient. Both third- and fourth-order R–K schemes were implemented and found to produce similar results. The linear viscous terms were integrated exactly using an integrating factor approach. The time step size was chosen automatically by the code to keep the CFL number within the numerical stability bounds for the particular scheme being used.[33]

Test of the code included verifying its ability to predict the linear stability of the primary base flow. For value of Ω below Ω_c it was found that perturbations died rapidly while just beyond Ω_c steady cellular patterns developed that agree with those of other authors.[16,17]

Two types of dealiasing were tried during the course of the simulation as were spatial grids of double the resolution (64×64 as oppose to 32×32). These alternations did not significantly change the computed results. On the other hand, attempts to use 16×16 spatial grid gave rise to underresolved flows that were drastically different in nature. The results reported here are for 32×32 spatial grid (i.e., we integrated 1024 ordinary differential equations), which was found adequate for the parameter range (25). All runs were allowed to settle for a considerable time (5000 + time units) before any data were recorded.

IV. TOOLS OF THE ANALYSIS

Here we briefly comment on the tools used in the analysis of the direct numerical simulation of the Kolmogorov flow. The tools needed for the investigation can be grouped according to their function.

A. Temporal power spectra

We need some mathematical tools to distinguish between chaotic and quasiperiodic regimes of the flow. The temporal power spectra (PS) are indispensable for this purpose.[36]

Let PS $(\gamma(t))$ denote the temporal PS of the time signal $\gamma(t)$. It follows from Eq. (18) that there are $32^2 = 1024$ individual time histories available for the use in the temporal PS. For the problem at hand, we define the energy PS box averaged per m_1 wave number in x direction as (modulo a multiplicative normalization)

$$\mathrm{PS}(\mathbf{u})^{(m_1)} = \sum_{m_2} \mathrm{PS}(\mathrm{Re}[u_{(m_1,m_2)}(t)]) + \mathrm{PS}(\mathrm{Im}[u_{(m_1,m_2)}(t)]). \tag{26}$$

In other words, we take the temporal PS of all the time histories resulting from the projections onto basis function (17) which include m_1 in the wave-number pair $\mathbf{m} = (m_1,m_2)$ and average over them. This is in keeping with the definition of the PS of a time stationary signal as being the Fourier transform of the autocorrelation. In the calculations we frequently set m_1 to zero and use the resulting temporal power spectrum to distinguish between chaotic and quasiperiodic regimes of the flow.

For later reference we remark now that since the PS is the Fourier transform of the autocorrection it follows that as the frequency $|f| \to \infty$ the PS vanishes faster than any inverse power of $|f|$. This is a simple consequence of the fact that in any numerical simulation we are integrating a system

of ordinary differential equations with smooth direction fields and hence the solution is C^∞ in the time variable.

B. Poincaré sections

We use Poincaré sections to study geometrical structure of the attractor and to qualitatively discuss its degree of complication. Methods for the calculation of these sections have been given by Keefe[5] and others. The phase space employed in the calculation of the Poincaré sections is spanned by the spatial Fourier modes of the solution $\mathbf{u}(\mathbf{x},t)$,

$$\mathbf{u}(\mathbf{x},t) = \sum_{\mathbf{m}} u_{\mathbf{m}}(t)\mathbf{B}_{\mathbf{m}}(\mathbf{x}), \tag{27}$$

where $\mathbf{u}_{\mathbf{m}}$ and $\mathbf{B}_{\mathbf{m}}$ are complex.

The choice of the sectioning plane for the Kolmogorov flow becomes very important, for it determines which attractor features are covered by the study. Here, we are mainly concern with the visual structure of the attractor itself. CPU expenditures to accumulate a large enough collection of points for a highly resolved Poincaré section become considerable. Therefore a need arises for the use of the discrete symmetry group of the flow to extend the available data. This in turn suggests that some care should be exercised in the choice of a sectioning plane. In particular, an acceptable choice is a plane that is invariant under the symmetry groups (both discrete and continuous). It is also a good practice to choose as a section, a plane for which the flow projections maximize the energy contained in the basis function $\mathbf{B}_{\mathbf{m}}(\mathbf{x})$ with respect to the L^2 norm. With that in mind, we take the forcing function plane

$$\mathrm{Im}(u_{(0,4)}) = D, \tag{28}$$

$$\mathrm{Im}(\dot{u}_{(0,4)}) > 0, \tag{29}$$

as our invariant under the action of the symmetry group section plane for the Poincaré sections used later. The choice of the constant D controls apparent positioning of the hyperplane in the phase space and is dependent upon Ω. In actual calculations, we consider a series $\{\mathrm{Im}[u_{(0,4)}(t_i)]\}_{i=1}^{N}$ of snapshots of the variable $\mathrm{Im}[u_{(0,4)}(t)]$. We then set D to its average, i.e.,

$$D = \frac{1}{N}\sum_{i=1}^{N} \mathrm{Im}[u_{(0,4)}(t_i)]. \tag{30}$$

The Poincaré sections shown in the later sections plot the $\mathrm{Re}(u_{(0,1)})$ vs $\mathrm{Im}(u_{(0,1)})$.

For further reference, we note here representation of the symmetry group (13), (14) in terms of the spectral components of $\mathbf{u}(\mathbf{x},t)$. It $\mathbf{u}(\mathbf{x},t)$ is represented as in (27) then the glide reflection $g\mathbf{u}(\mathbf{x},t)$ (13) can be written as

$$g\mathbf{u}(\mathbf{x},t) = \sum_{\mathbf{m}} -u_{(-m_1,m_2)}(t)e^{i(m_2/n)\pi}\mathbf{B}_{\mathbf{m}}(\mathbf{x})$$

$$= \sum_{\mathbf{m}} u^*_{(m_1,-m_2)}(t)e^{i(m_2/n)\pi}\mathbf{B}_{\mathbf{m}}(\mathbf{x}), \tag{31}$$

while the rotation $R\mathbf{u}$ (14) is

$$R\mathbf{u}(\mathbf{x},t) = \sum_{\mathbf{m}} u_{-\mathbf{m}}(t)\mathbf{B}_{\mathbf{m}}(\mathbf{x}) = \sum_{\mathbf{m}} -u^*_{\mathbf{m}}(t)\mathbf{B}_{\mathbf{m}}(\mathbf{x}). \tag{32}$$

It then follows from (30)–(32) that our sectioning plane is invariant under the symmetry group of the flow.

From the examination of Eq. (32), it is apparent that the rotation corresponds to the reflection around the imaginary axis for any variable $u_{\mathbf{m}}(t)$. On the other hand, glide-reflection action (31) of the symmetry group on $u_{(0,1)}(t)$ gives

$$-u_{(0,1)}(t)e^{i(\pi/4)}. \tag{33}$$

This corresponds to $\frac{5}{4}\pi$ rotation in the $\mathrm{Re}[u_{(0,1)}(t)]$-$\mathrm{Im}[u_{(0,1)}(t)]$ plane. Thus the discrete symmetry group of the flow induces extra symmetries onto the $u_{(0,1)}(t)$ plane. They correspond to the reflection around the $[(1+2i)/8]\pi$, $i=0,1,2,3$ axis. These symmetries figure prominently in the discussion of the results of our numerical simulation.

C. Lyapunov spectrum

All of the mathematical tools mentioned above can indicate the presence of chaos in the dynamical system, but do not directly address the level of randomness present, or how chaotic a solution is.

For these purposes, we compute the Lyapunov exponents for the two-dimensional Navier–Stokes equations (8)–(10) and these in turn allowed us to compute the dimension of the attracting set of the chaotic flow. We write the governing system in symbolic form as

$$\frac{d\mathbf{u}}{dt} = \mathcal{F}(\mathbf{u}), \tag{34}$$

and denote a reference or fiducial trajectory by $\mathbf{u}^0$. If an initially nearby trajectory is written as

$$\mathbf{u} = \mathbf{u}^0 + \epsilon\mathbf{v} \tag{35}$$

then in the limit $\epsilon \to 0$, $\mathbf{v}$ satisfies the variational equation,

$$\frac{d}{dt}\mathbf{v} = \mathcal{L}(\mathbf{u}^0)\mathbf{v}, \tag{36}$$

where

$$\mathcal{L}(\mathbf{u}^0) = \frac{\delta\mathcal{F}(\mathbf{u}^0)}{\delta\mathbf{u}^0} \tag{37}$$

is easily obtained through the linearization.

The largest Lyapunov exponent is defined as the maximum exponential rate at which nearby trajectories diverge

$$\lambda_1 = \lim_{\tau\to\infty}(1/\tau)\ln\|\mathbf{v}(\tau)\|. \tag{38}$$

Thus the idea of a Lyapunov exponent can be regarded as a generalization of the stability exponent of an equilibrium solution, and finding a positive Lyapunov exponent is an unambiguous signature of a chaos.

It is to be expected that all initial data $\mathbf{v}(\mathbf{x},0)$ for the linear problem (36) will rapidly evolve in the direction of the greatest growth. Using this fact, it is relatively easy to compute λ_1 by integrating (36) with arbitrary initial data. However, it is not quite so trivial to obtain other members of the Lyapunov spectrum. Algorithms for calculating these have been given by Bennetin *et al.*,[37] Shimeda and Nagashima,[38] and Wolf *et al.*,[39] and are further explained by Fitzmaur-

ice.[40] The essence of the trick lies in computing volumes of infinitesimal ellipsoids. In fact if $\epsilon_n(\tau)$ denotes the volume of an n ellipsoid in phase space it then follows that

$$\lambda_1 + \lambda_2 + \ldots + \lambda_n = \lim_{\tau \to \infty} (1/\tau) \ln \epsilon_n(\tau). \tag{39}$$

Thus after (38) one calculates $\lambda_1 + \lambda_2$, then $\lambda_1 + \lambda_2 + \lambda_3$, etc., and thereby the spectrum $\lambda_1, \lambda_3, \ldots$.

Since the system in question is dissipative we know that the sum (39) will become negative for n large enough. And since it is chaotic it must be positive for $n = 1$. Therefore this sum must cross zero at some point as one increases n. One may then use the formula of Kaplan and Yorke,[22]

$$d_L = N - \Sigma_k \lambda_k / \lambda_{N+1}, \tag{40}$$

to estimate the dimension, d_L, of the attractor where N is the largest integer for which the sum is positive. Constantin *et al.*[41] have shown that the Kaplan–Yorke formula gives an upper bound for the Hausdorf dimension.

The original nonlinear code for computing the fiducial trajectory (34) was adapted to simultaneously compute the linearized system (36). For each Lyapunov exponent calculated one essentially computes a trajectory (36) from a fresh initial conditions. We note that while (36) is linear, it has nonconstant coefficients, and, from a computational point of view, is as costly as the original system (34). Thus, Lyapunov spectrum calculations are very expensive.

One test of the code was easily carried out, namely by choosing u^0 to be primary base flow (21). We could compute a λ_1 that should, indeed, agree with the most unstable eigenvalue computed from the Orr–Sommerfeld equations using the same base flow.

In the chaotic regime we tested Lyapunov code by varying the order of the time-stepping scheme (R–K 3 and R–K 4), by varying the spatial resolution (32×32 and 64×64), and by trying many different initial conditions for the linearized systems. None of these changes altered the Lyapunov dimension value in the first decimal digit. So we report values here to that accuracy.

V. RESULTS

In this section we present the results of our direct numerical simulation of the Kolmogorov flow. We have found that there are two main regimes of the flow corresponding to different ranges of the bifurcation parameter Ω. Tentatively these are termed as being the regimes of small and large scale structures. Explanation for this terminology will be evident from the streamline plots to be discussed.

A. Small scale structures

1. $0 < \Omega/\Omega_c \leqslant 1$

In this range the asymptotic solution of the N–S equations (8)–(10) is the fixed point (21). Streamlines and vorticity plots for the parallel shear flow in horizontal direction are shown in Fig. 1. Computations using arbitrary initial conditions rapidly decayed into this pattern and all computed Lyapunov exponents were negative, indicating the linear stability of this state.

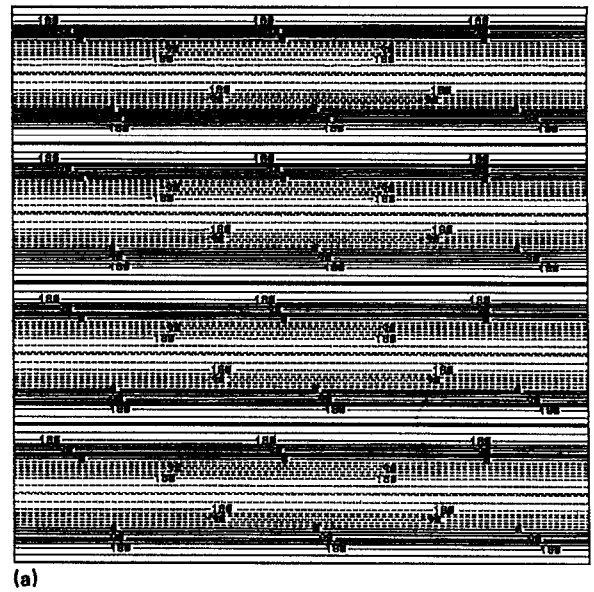

FIG. 1. Parallel shear layer flow corresponding to the fixed point solution at $\Omega = 0.5\Omega_c$: (a) streamlines, (b) vorticity.

2. $1 < \Omega/\Omega_c < 1.97$

As we increase Ω, the horizontal shear flow becomes unstable and the flow pattern changes. At $\Omega/\Omega_c = 1$, the parallel shear flow bifurcates to a new solution. In this range the motion is steady and purely cellular and illustrations of this are shown in Figs. 2 and 3. It is interesting to note that at the lower range of the parameter Ω the flow is almost horizontal [Fig. 2(a)] while at higher values of Ω in this range the motion is mainly in the vertical direction [Fig. 3(a)] with well defined cells. In the first instance the saddle points of the separatrices of the streamlines are formed horizontally while in the latter case they are joined vertically. This is in an agreement with the experiments of Bondarenko *et al.*[42] for a magnetohydrodynamic problem under similar forcing. Lyapunov exponents in this range were found to be negative but

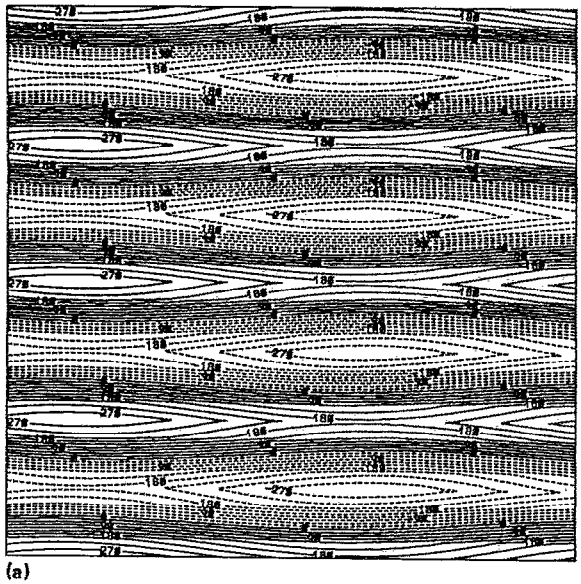

(a)

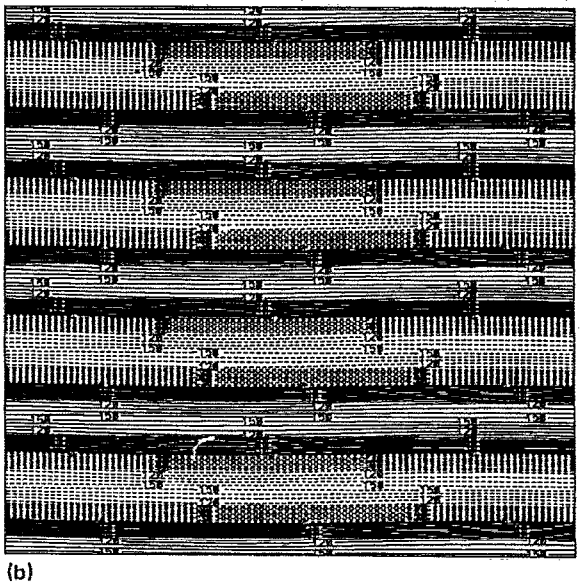

(b)

FIG. 2. Steady cellular flow found at $\Omega = 1.12\Omega_c$ with the motion mainly in the horizontal direction: (a) streamlines, (b) vorticity.

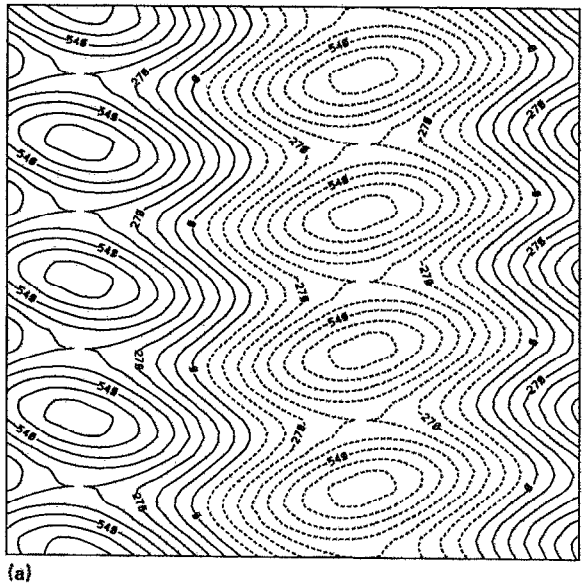

(a)

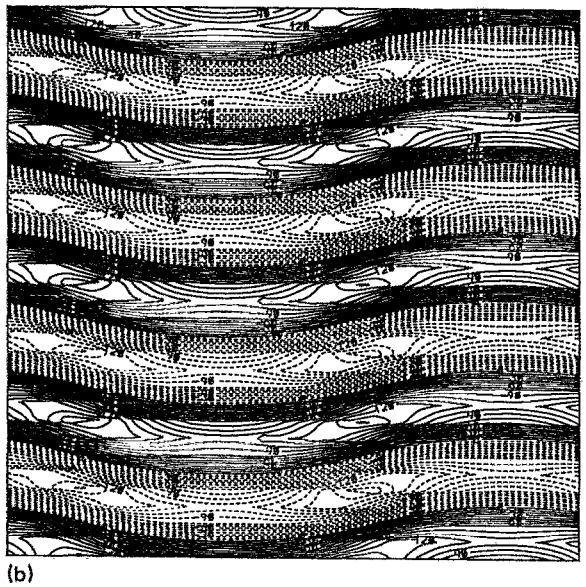

(b)

FIG. 3. Steady cellular flow found at $\Omega = 1.5\Omega_c$ with the motion mainly in the vertical direction and the fastest growing perturbation has wave number 1 in the horizontal direction: (a) streamlines, (b) vorticity.

of small absolute magnitude indicating that the cellular pattern is only weakly linearly stable.

3. $1.97 \leqslant \Omega/\Omega_c \leqslant 2.2$

In this range the flows still have the steady cellular structure but the number of cells in the horizontal direction had suddenly doubled. The new flow patterns are depicted in Fig. 4. One can explain this phenomena by noting that in this range the horizontal wave number of the fastest growing mode changes from 1 to 2 (first observed by Green[16]). A very important feature of the flow in this and previous ranges is that it is invariant under the discrete symmetry group transformations. By invariance we mean that for any transformation g in the discrete symmetry group of the flow there is $0 \leqslant l \leqslant 2\pi$ such that

$$T_l g\mathbf{u} = \mathbf{u}, \tag{41}$$

where T_l is a translation by l in x direction and $\mathbf{u}$ is a solution of N–S equations (8)–(10). In other words, we say that the flow is invariant under the discrete symmetry group if, after application of any transformation from the discrete symmetry group to the flow, we can translate the transformed flow in the horizontal direction in such a way that it coincides with the original flow.

We conducted a search for hysteresis effects in this range of the parameter space. The search for the reverse hysteresis in this range of the parameter space Ω to the previous range was unsuccessful, while the search for the forward hysteresis in the range $1 < \Omega/\Omega_c < 1.97$, reveals that the in-

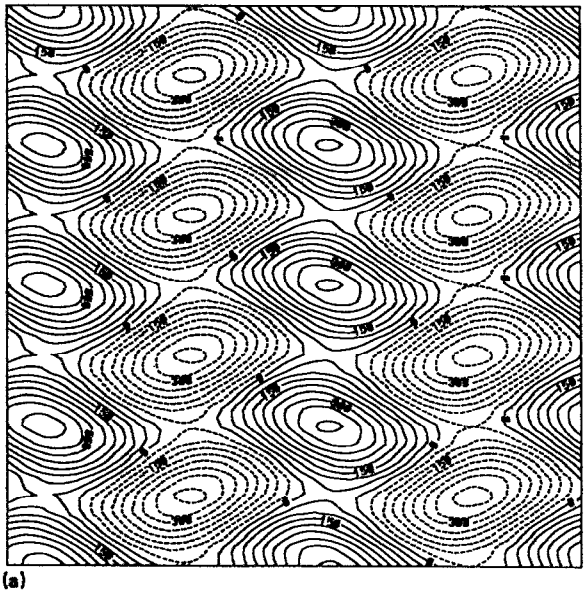

(a)

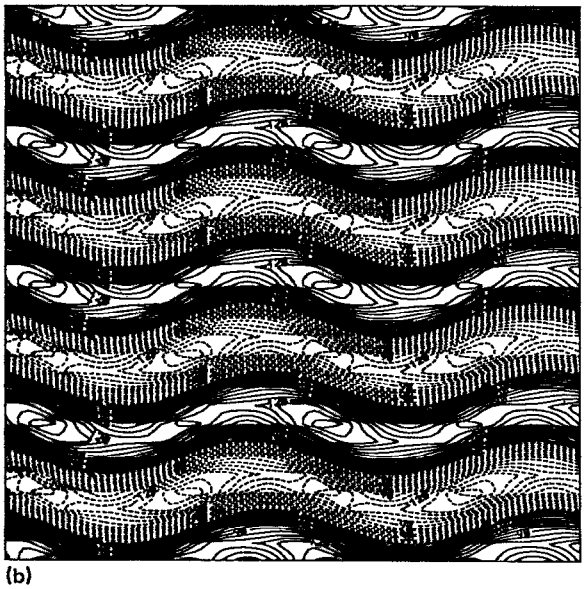

(b)

FIG. 4. Steady cellular flow found at $\Omega = 2\Omega_c$ with the motion mainly in the vertical direction and the fastest growing perturbation has wave number 2 in the horizontal direction: (a) streamlines, (b) vorticity.

variant flow under the discrete symmetry group transformations persists until the parameter Ω reaches $2.2\Omega_c$. For $\Omega > 2.2\Omega_c$, it gives way to a flow similar to one discussed in the next range of the parameter space Ω with the following exceptions: number of cells in the streamline plot is halved in the x direction; and there is a steady horizontal drift developing in the flow. The speed of the drift approaches to zero at $\Omega = 2.2\Omega_c$.

4. $2.2 < \Omega/\Omega_c < 3.53$

As Ω increases, small amplitude perturbations at the saddle points of the streamlines will grow and lead to the eventual breakdown of the steady cellular pattern depicted in Figs. 2–4. At $\Omega/\Omega_c = 2.2$ another bifurcation in parameter space takes place. For the range under discussion there is a gradual breakdown in the symmetry of the flow that becomes more pronounced as the bifurcation parameter Ω reaches the upper end of the range. Unlike the first two bifurcations, linear stability theory as applied to the primary base flow (21) offers no clues for the forms that are obtained. The new flow patterns are depicted in Fig. 5, the features to note here are that the cells are no longer aligned on vertical lines and are of different size. It is perhaps remarkable that these cellular structures are still steady.

5. $3.53 \leqslant \Omega/\Omega_c \leqslant 3.6$

At $\Omega/\Omega_c = 3.53$ the asymptotic flow is no longer steady, but is statistically stationary, Now, the flow spends most of the time in the steady cellular state shown in Fig. 5. But from time to time, the flow is intermittently disturbed by

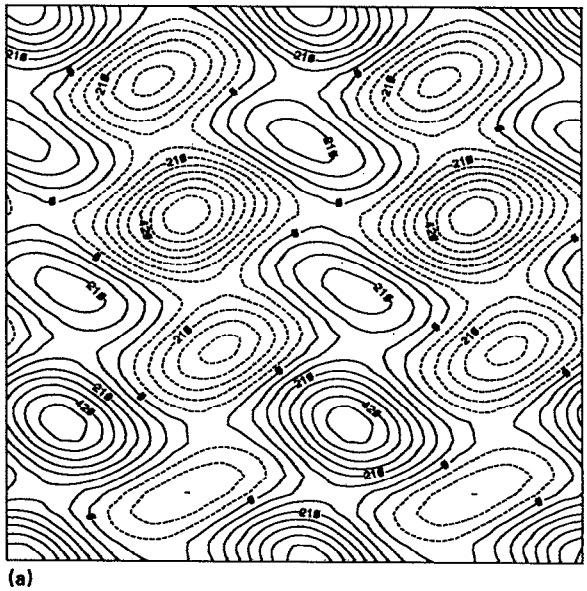

(a)

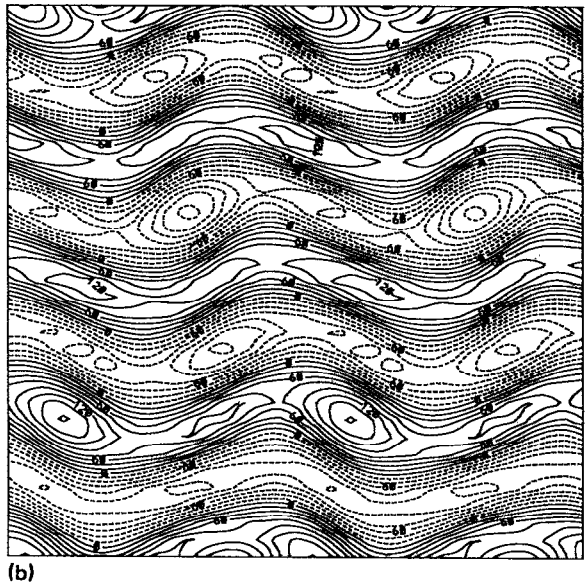

(b)

FIG. 5. Steady cellular flow found at $\Omega = 3\Omega_c$: (a) streamlines, (b) vorticity.

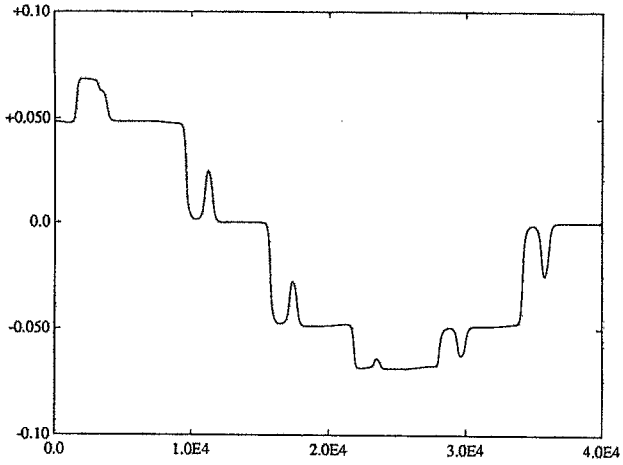

FIG. 6. Time series of $\mathrm{Re}(u_{(0,1)})(t)$ at $\Omega = 3.65\Omega_c$. Plateaus correspond to a steady cellular flow.

random horizontal shifts occurring on a very rapid time scale. the time between bursts is very long and is a decreasing function as the parameter Ω reaches the upper end of the range. Figure 6 shows the time series of $\mathrm{Re}(u_{(0,1)})$. Here, the plateaus correspond to a steady cellular state. After the horizontal shift, the cells oscillate with a small amplitude for a short while, and then settle down very rapidly to a steady pattern before undergoing the next horizontal shift. This state is chaotic but only over a very long time scale, i.e., the Lyapunov spectrum has some very small positive exponent. This may be related to the heteroclinic connections of Armbruster *et al.*[43] and Aubry *et al.*[44]

6. $3.6 < \Omega/\Omega_c < 4.47$

In this range the nature of the flow changes once again. We now find periodic oscillations occurring in the cellular structures as depicted in Fig. 5. Also, the solution develops a slow drift in the horizontal direction, but without a net transport off mass. The drift may be regarded as the wave motion. It also follows from symmetry that the drift wave can move in either direction. We conclude from Fig. 7, which shows the temporal power spectrum, that there is a principal frequency, the large peak, and subharmonic frequencies of it present in the flow. These correspond to the oscillations of the pattern around larger vortices and inner oscillations of the vortices themselves. It is interesting to note that we have found no regime of the flow when only the principal frequency is present.

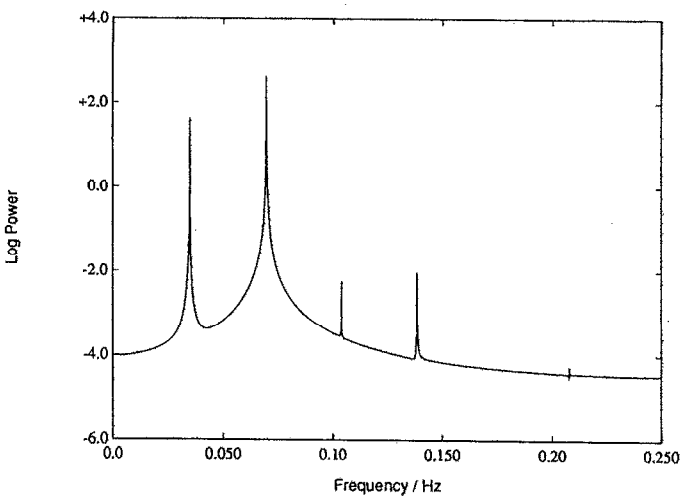

FIG. 7. Power spectrum of the velocity u at $\Omega = 4\Omega_c$. The principal frequency and its subharmonic dominates the spectrum.

7. $4.47 \leqslant \Omega/\Omega_c < 4.58$

Now, the flow enters its second chaotic regime. Figure 8 depicts a typical time series of the signal $\mathrm{Re}(u_{(0,1)})$ in this range, from which we conclude that the chaos is intermittent. Examining the power spectrum shown in Fig. 9, we see that the principal and subharmonic frequencies are prominently present in what is a broadband spectrum. We did not attempt to calculate the Lyapunov dimension for the dy-

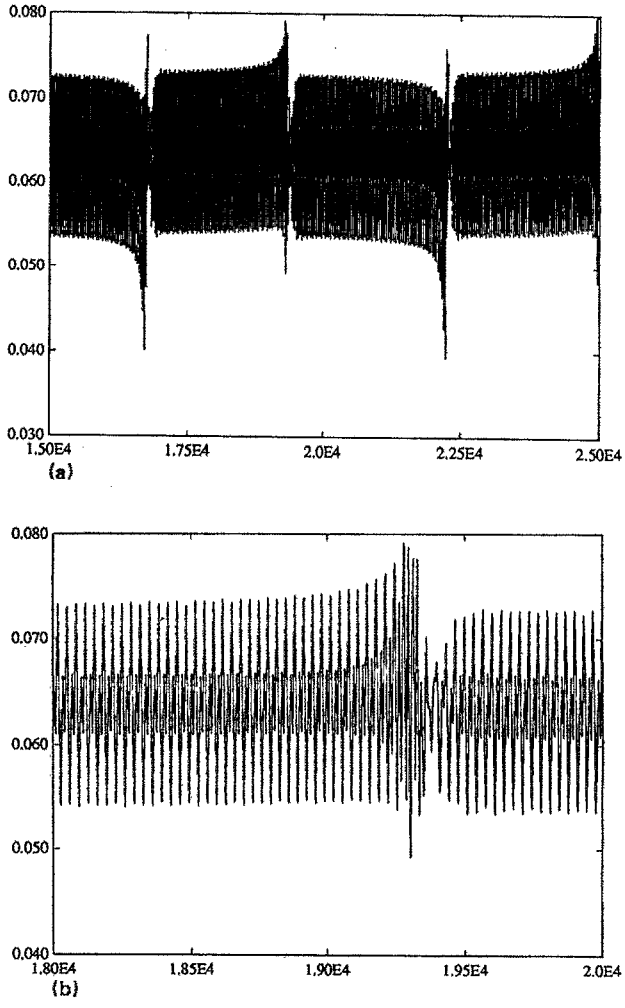

FIG. 8. (a) Time series of $\mathrm{Re}(u_{(0,1)})(t)$ at $\Omega = 4.48\Omega_c$, (b) blowup of (a). The flow is intermittent chaotic with long time intervals between the bursts of activity.

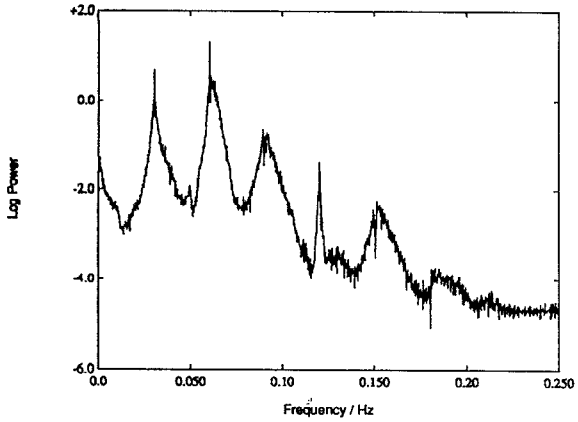

FIG. 9. Power spectrum of the velocity u at $\Omega = 4.48\Omega_c$. The flow is chaotic, but the principal frequency and its subharmonics still dominate the spectrum.

namical system in this range of Ω because of the very long time interval between the bursts of activity in the flow. A most remarkable feature of the flow in this range is that the chaotic attractor is *not unique*! The dynamical system has several chaotic attractors each with its own basin of attraction lying quite close to the fixed point (21). On the basis of extremely long calculations we conclude that these attractors are not connected. Figure 10 shows the Poincaré section depicting cuts of the chaotic attractors. Two darker points in the blown up section [Fig. 10(b)] correspond to the punctures produced by the solution in the laminar phase of the intermittency. In actual calculations we obtain only one of the attractors (depending on the chosen initial data), and the rest are obtained by using the discrete symmetry group. Alternatively, we can apply the symmetry group to the initial data and thus generate each of the attractors. This was in fact done to further verify our computational scheme. Another peculiarity of the flow is that there are only eight symmetric attractors instead of 16 as predicted by the discrete symmetry group. This happens because the action of five glide reflections followed by the rotation by π applied to the solution maps the attractor onto itself. This induces an extra symmetry into the attractor corresponding to the reflection around the axis denoted by the dashed line in Fig. 10(b), as was discussed in the earlier part of this paper dealing with the Poincaré sections.

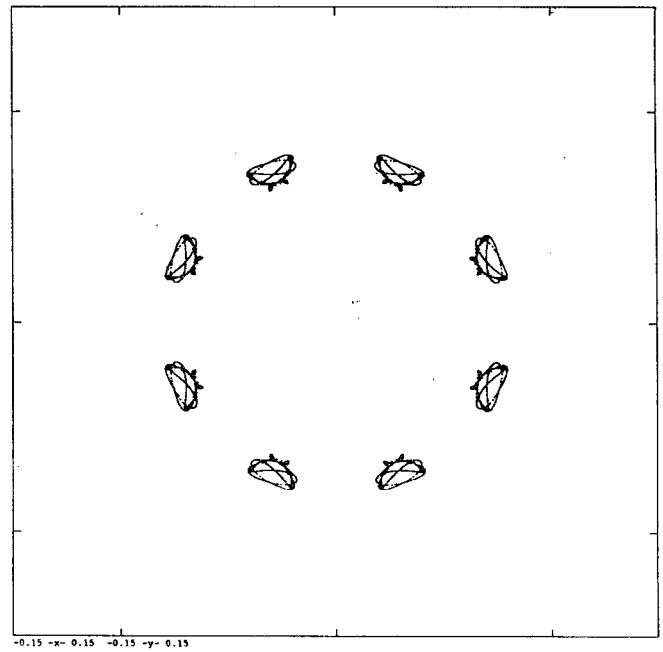

(a)

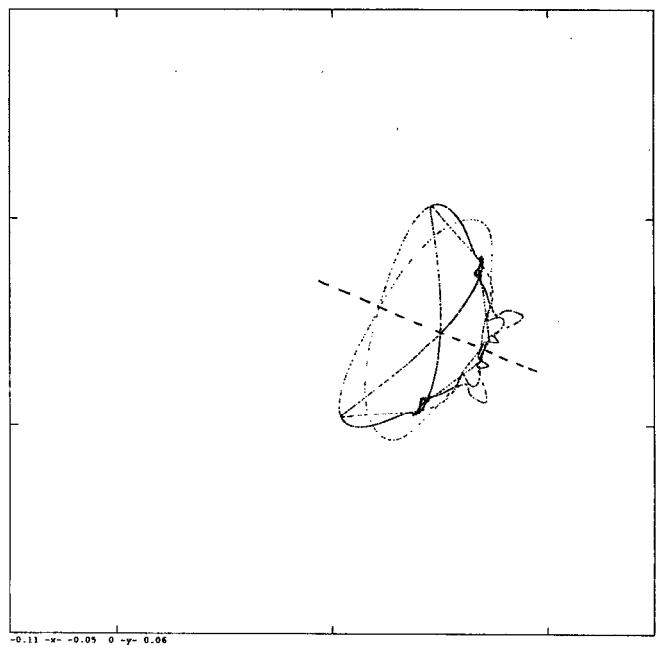

(b)

FIG. 10. (a) Poincaré section of the chaotic attractors at $\Omega = 4.48\Omega_c$. (b) One of the attractors. Attractors are not ergodic. A dashed line in (b) shows the axis of symmetry of the attractor.

8. $4.58 \leqslant \Omega/\Omega_c \leqslant 4.65$

As Ω increases, different symmetric attractors start intersecting each other and now the flow is intermittently chaotic with one ergodic attractor consisting of eight connected symmetric components. This is similar to *crisis-induced intermittency* discussed by Greboggi *et al.*[45] when a number of chaotic attractors in a system with symmetries merge to form a single attractor. This manifests itself by intermittent switching between behaviors characteristic of each of the attractors before merging. Figure 11 shows the time series of $\mathrm{Re}(u_{(0,1)})$. The evidence of the intermittent bursts is clearly present and sudden jumps correspond to the solution jumping to a different component of the attractor. We present the temporal power spectrum in Fig. 12. This new state is more chaotic than the previous case, but still there is evidence of the principal frequency from the lower parameter values. The Poincaré section is shown in Fig. 13 ("butterflies" section). Darker regions in the blown up section of the attractor in Fig. 13(b) correspond to the points where the solution spends most of the time between intermittent bursts. Moreover, comparing Figs. 13 and 10, we notice

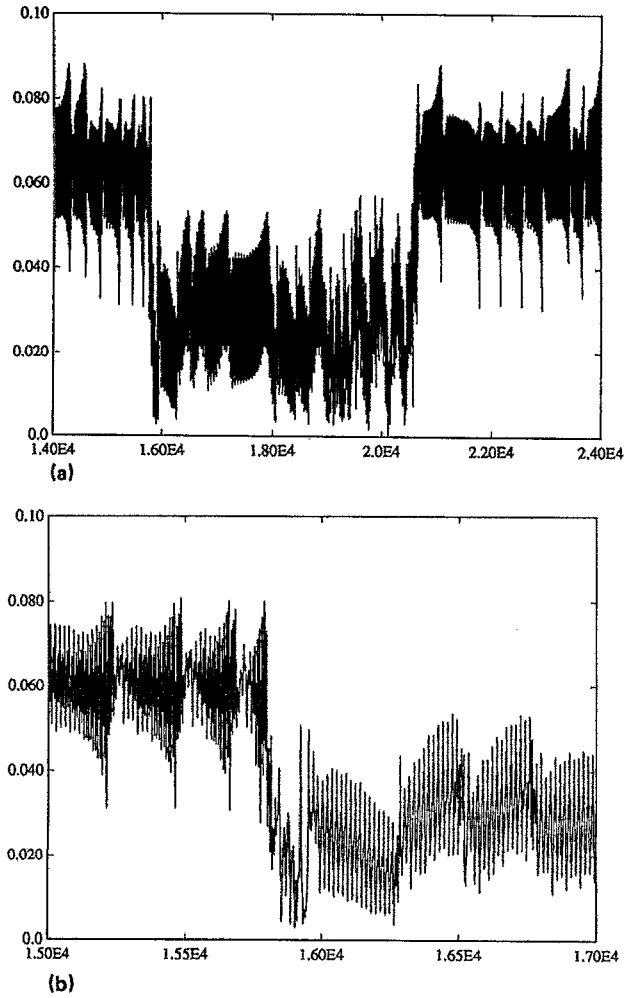

FIG. 11. (a) Time series of $\mathrm{Re}(u_{(0,1)})(t)$ at $\Omega = 4.63\Omega_c$, (b) blowup of (a). The flow is intermittent chaotic. The sudden jumps correspond to the solution jumping from one component of the chaotic attractor to another.

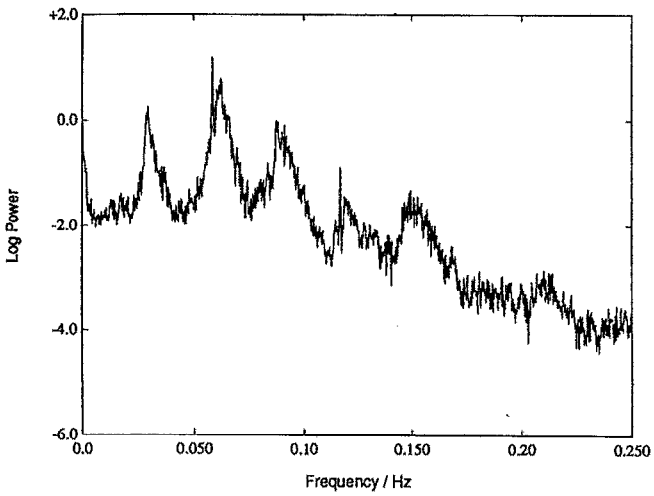

FIG. 12. Power spectrum of the velocity u at $\Omega = 4.63\Omega_c$.

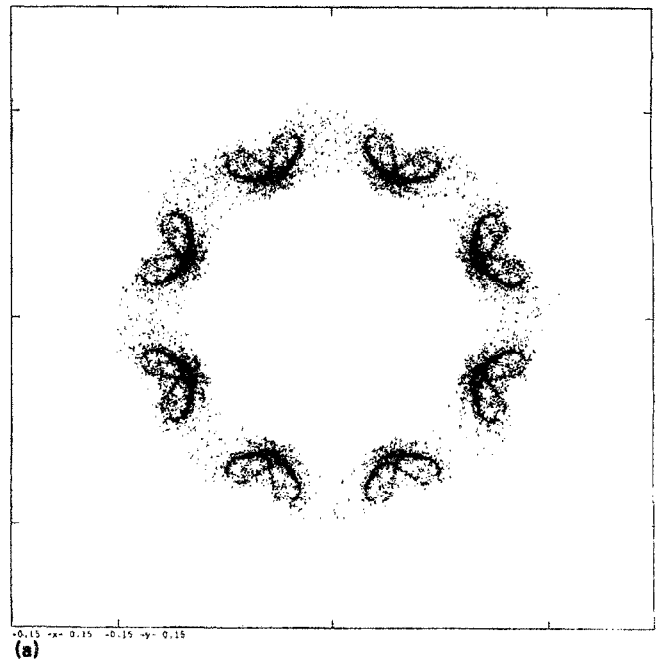

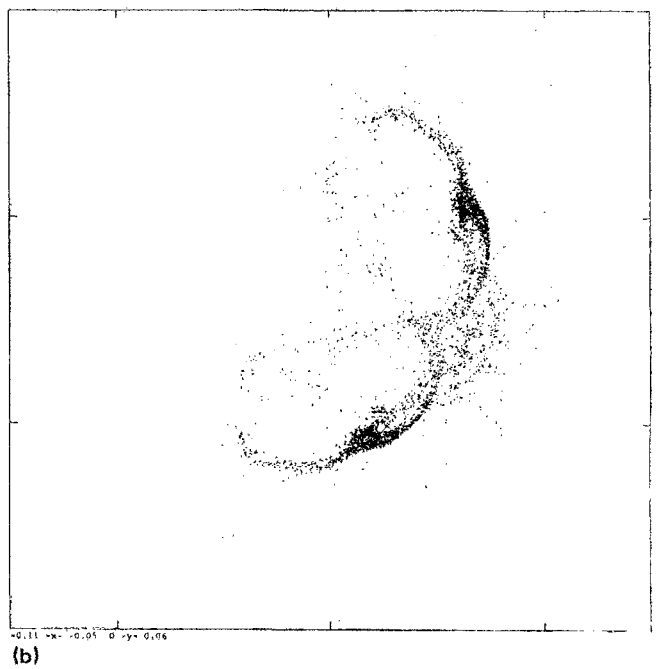

FIG. 13. (a) Poincaré section of the chaotic attractor at $\Omega = 4.63\Omega_c$. (b) One of the components of the attractor. Flow intermittently jumps from one component of the attractor to another.

that the main features of the nonunique attractor are still present.

9. $4.65 < \Omega/\Omega_c \leqslant 4.71$

Another remarkable feature of the Kolmogorov flow is, that counter to intuition, the parameter space Ω contains windows of relaminarization between different chaotic ranges of the flow. This range is an example of one of such windows. Here, the flow returns to a periodic regime with a

principal and subharmonic frequencies in the power spectrum. Again, there is no regime with just the principal frequency is present without subharmonics. This flow is similar to the range $3.6 < \Omega/\Omega_c < 4.47$. It also, develops a slow steady drift in the horizontal direction. We also note that this drift appears to vanish in the chaotic windows of the flow.

At $\Omega = 4.72\Omega_c$ we see the formation of large scale structures.

B. Large scale structures

Although we are mainly interested in the asymptotic behavior of the Kolmogorov flow, it is of interest to examine how the large scale structures are formed. The process is basically the same for all values $\Omega \geqslant 4.72\Omega_c$.

We start with a small perturbation of the fixed point flow (21). This state persists for roughly the time scale predicted by the linear stability analysis. Then on a very rapid time scale the flow changes to the unsteady cellular pattern of the sort illustrated in Fig. 5. This state with many small cells persists for a very short time and then the flow plunges into chaos. The new state is vigorously chaotic, characterized by the rapid movements of a small vortical structures, a snapshot of which is shown in Fig. 14. By a rough count it is seen that the same number of vortical structures appears in Figs. 5 and 14. We refer to this state as *metastable* or *transient* chaos following the terminology of Grebogi *et al.*[46] As seen by Basdevant *et al.*[47] and Benzi *et al.*[48] in studies of two-dimensional turbulence, vortical structures persist and intermittency is marked. Of all the chaotic states observed in our numerical experiments, this is the only state that can be called chaotic both spatially and temporally and hence is turbulent according to common convention. At the lower

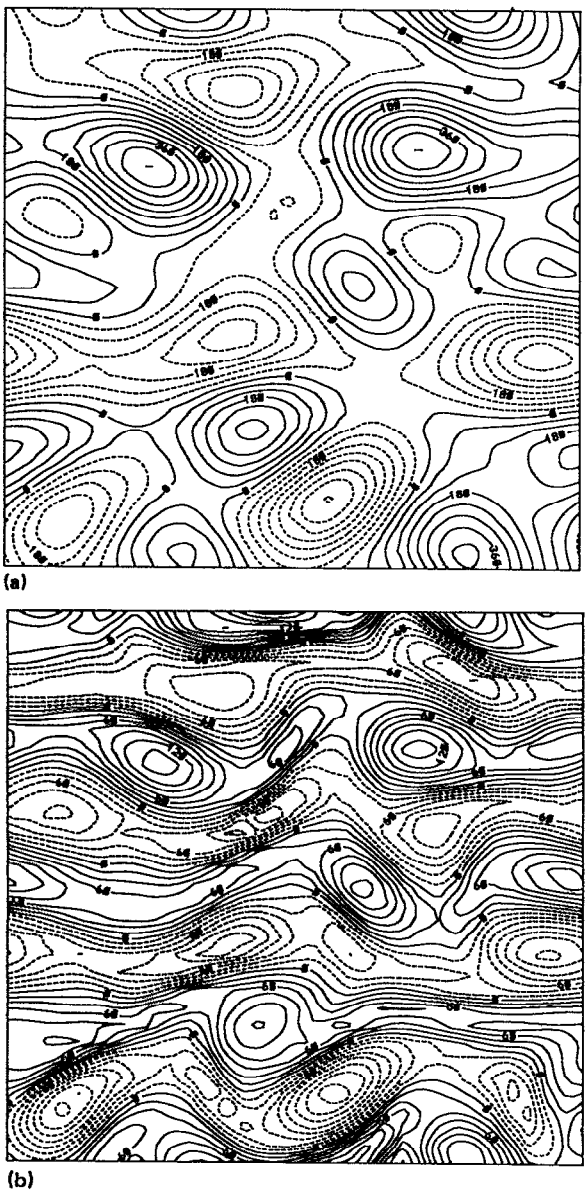

FIG. 14. Instantaneous flow pattern found in the metastable chaotic regime at $\Omega = 10\Omega_c$: (a) streamlines, (b) vorticity. The flow is both spatially and temporally chaotic, and thus may be called turbulent.

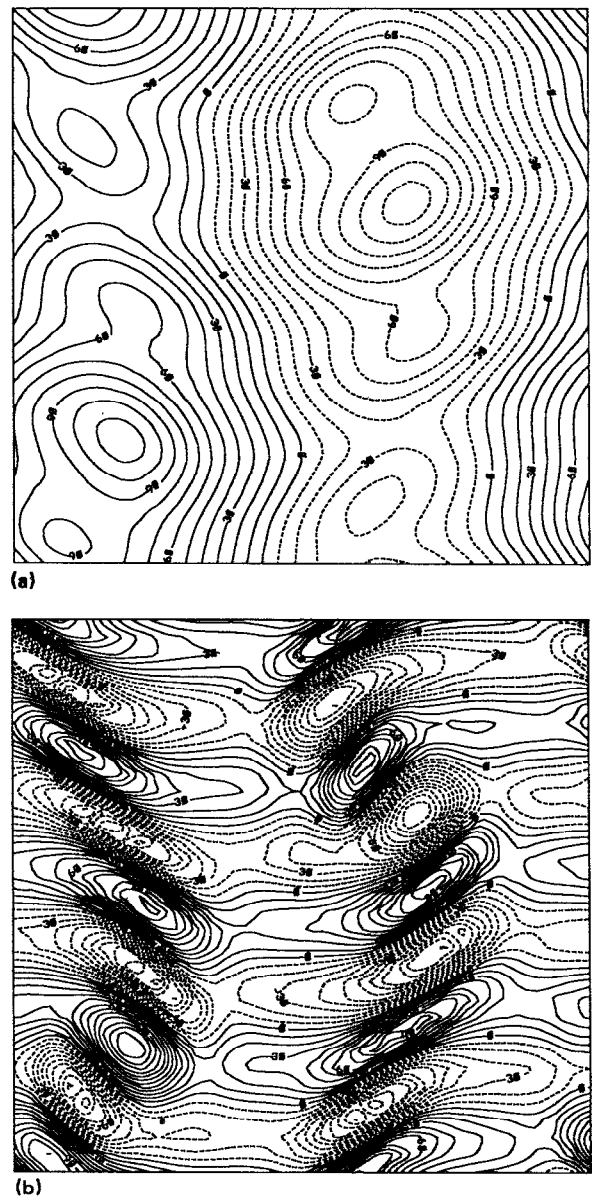

FIG. 15. Steady spatially chaotic flow found at $\Omega = 5.9\Omega_c$: (a) streamlines, (b) vorticity. Also, this is an example of large scale structures.

range of Ω this *metastable* chaos holds for a relatively long time, while at a higher values of the bifurcation parameter Ω it can be extremely short.

In any case the phase point finds an escape hole in the metastable attractor and we eventually see the formation of large scale structures such as those depicted in the Fig. 15. The new attractor is stable. Considerable vortex merging has taken place in passing from Fig. 14 to Fig. 15. The two large structures shown in the streamline plot of Fig. 15(a) are somewhat misleading. On a closer examination of the vorticity plot, we see that we have roughly the same number of distinct vortices as before and that the large structures in the streamline plot consist of a number of a counter-rotating vortices. These new large scale structures are completely different from the small scale structures that we dealt with in the previous subsection. Examining the vorticity plot shown in Fig. 5(b), we notice that at the small scales the vortices are arranged in a lattice. Thus, the unsteady small scale structures flow can be considered as oscillations or "breathing" of the lattice structure. In the *metastable* regime this lattice structure is broken, and we have a soup of vortices moving randomly around. Later the vortices merge together and arrange themselves on a curved line with two vortices containing most of the circulation. These vortices correspond to the eyes of the large scale structures depicted in the streamline plot of Fig. 15(a). It is of interest to note here that the vertical position of the eyes of the large scale structures are at hyperbolic points of the forcing functions when the flow is not chaotic.

A search for the hysteresis in the range of the large scale structures regime to the small scale structures regime was performed by making runs in reverse in the parameter space Ω, starting on the previously converged attractor. It was observed that the large scale structures flow connects to the small scale structures flow at $\Omega = 2.2\Omega_c$. This small scale structures flow is invariant under the discrete symmetry group transformations, and it is the same as the flow in $1 < \Omega/\Omega_c < 1.97$ range. While in the reverse hysteresis loop in the range of the large scale structures to the small scale structures regime all chaotic and periodic regimes of the small scale structures flow have been bypassed. The flow in the hysteresis is somewhat similar to the flow in the $2.2 < \Omega/\Omega_c < 3.53$ range except that the number of cells in the x direction of the streamline plot is halved, and there is a steady horizontal drift present in the flow.

We will now describe in detail the bifurcations occurring in the large scale structure regime of the flow.

1. $4.72 \leqslant \Omega/\Omega_c < 5.9$

In this range the flow is periodic with one frequency. In addition, there is a horizontal drift present in the solution as also noted by She.[26] As Ω/Ω_c approaches 5.9 both the frequency of oscillations and drift speed approach zero simultaneously. Figure 16 shows the temporal power spectrum.

2. $\Omega = 5.9\Omega_c$

At $\Omega = 5.9\Omega_c$, the flow reaches the steady, spatially disorganized state depicted in Fig. 15. This was the only value

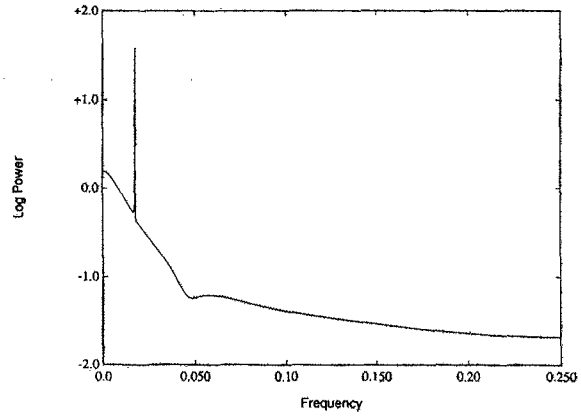

FIG. 16. Power spectrum of the velocity u at $\Omega = 5\Omega_c$. Only one frequency is present in the problem.

of the parameter Ω found by us where both the frequency of the oscillations and the drift speed are zero. The flow is chaotic only in the spatial domain!

3. $5.9 < \Omega/\Omega_c < 9.47$

As we start increasing Ω further, the flow develops both periodic oscillations and a slow drift in the horizontal direction. The direction of the drift changes according to the particular attractor the flow settles on. Moreover, as Ω increases, so does the drift speed and frequency of the oscillations. The periodic oscillations can be described as the "breathing" in the inner shells of the large scale structures. At $\Omega = 9.042\Omega_c$ a period doubling bifurcation takes place in the oscillations of the inner structures. Now the principal and subharmonic frequencies correspond to the breathing of the large scale structure itself and the oscillations of the inner shells. This regime persists up to $\Omega = 9.45\Omega_c$, where another period doubling bifurcation in the oscillations takes place. We can see clearly the principal and subharmonic frequencies in Fig. 17 showing the temporal power spectrum of the flow.

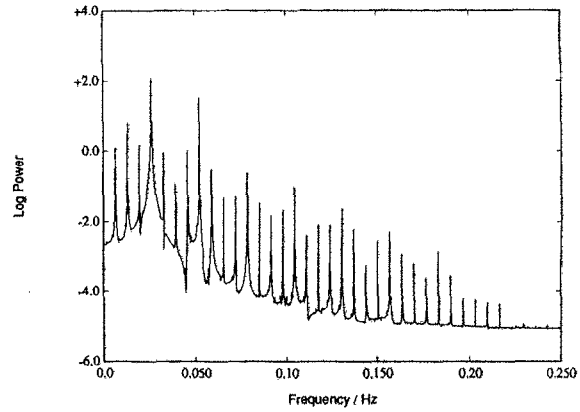

FIG. 17. Power spectrum of the velocity u at $\Omega = 9.458\Omega_c$. Two period doublings have taken place.

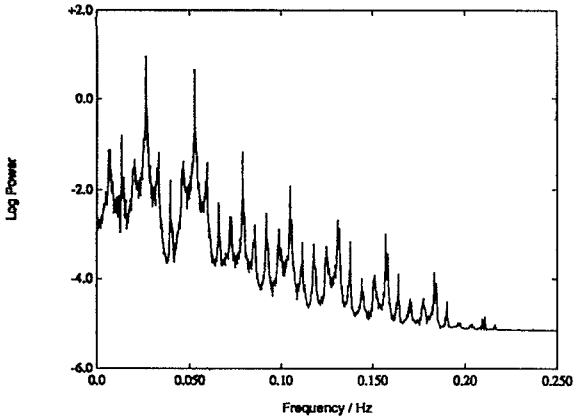

FIG. 18. Power spectrum of the velocity u at $\Omega = 9.47\Omega_c$. The flow is chaotic, but the principal frequency and its subharmonics are still dominant in the spectrum.

4. $9.47 < \Omega/\Omega_c < 9.66$

At $\Omega = 9.47\Omega_c$ the flow enters another chaotic regime which continues until Ω reaches $9.66\Omega_c$. We again find the remarkable feature in this window that there is chaos but that the attractors are *nonunique*! Here, the chaos is present in the irregular breathing-like oscillations of the inner structures that induces random oscillations of large scale structures. We observe in Fig. 18, which shows the temporal power spectrum, that the principal frequency and its subharmonics still dominate the motion. Horizontal drift diminishes to a trickle and sometimes changes directions. On average, there is no drift at all. Figure 19 depicts the Poincaré section of the attractor showing eight symmetric disconnected attractors. The slopes of the lines in Fig. 20 correspond to the values of Lyapunov exponents and the calculated Lyapunov dimension is 7.9.

5. $9.66 < \Omega/\Omega_c < 10.805$

At $\Omega = 9.66\Omega_c$ the flow enters another laminar window in the parameter space Ω. Here, the solution slowly drifts in the horizontal direction and has the principal and subharmonic frequencies. At $\Omega/\Omega_c = 10.4$ a period doubling bifurcation takes place. Figure 21 shows the temporal power spectrum at $\Omega = 10.7\Omega_c$.

6. $10.805 \leqslant \Omega/\Omega_c \leqslant 12.5$

As we increase Ω even further, the flow enters another chaotic regime at $\Omega = 10.805\Omega_c$. This flow now appears to be governed by an ergodic attractor which consists of eight symmetrical components and the solution intermittently jumps from one component to another. There is a very long time delay between successive jumps at Ω slightly greater than the 10.805, but it rapidly decreases as Ω increases. The principal frequency and its subharmonics dominate the power spectrum shown in Fig. 22. An examination of Fig. 23 showing the Poincaré section of the chaotic attractor, indicates that the components of the attractor have a fractal structure. The calculated Lyapunov dimension is 8.9. Another interesting point is that the direction of the drift

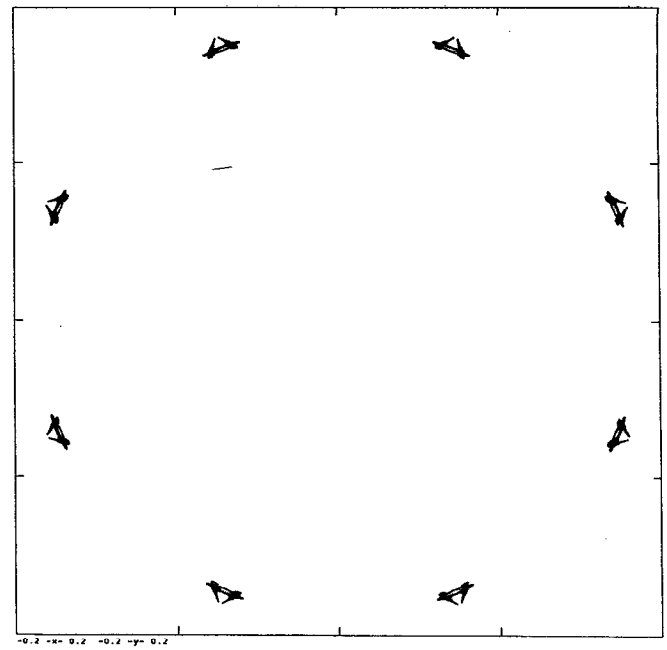

(a)

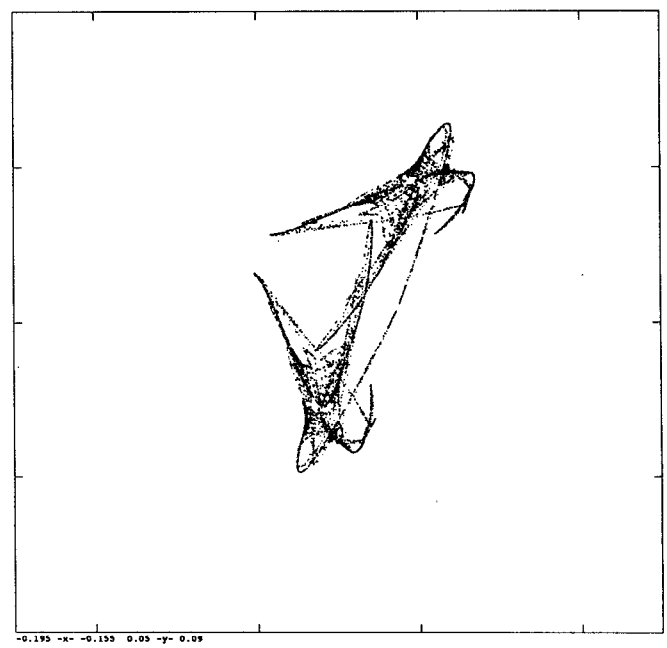

(b)

FIG. 19. (a) Poincaré sections of the chaotic attractor at $\Omega = 9.47\Omega_c$. (b) One of the chaotic attractors. Again, attractors are not ergodic.

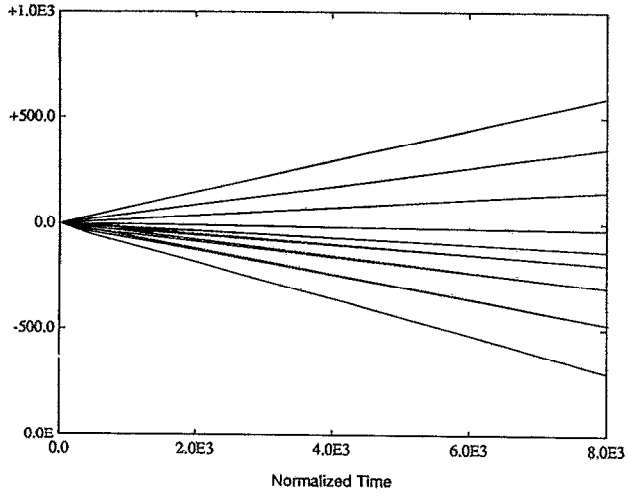

FIG. 20. Typical curves for the Lyapunov exponents calculations. Here $\Omega = 9.47\Omega_c$ and $d_L = 7.9$.

changes with each successive jump to a different component of the attractor.

As we continue to increase Ω, the different components of the chaotic attractor merge together and become indistinguishable. Nevertheless, the principal and subharmonic frequencies still dominate the temporal power spectrum shown in Fig. 24 for $\Omega = 12.5\Omega_c$. Now, the Lyapunov dimension increases to 10.8. Thus we might hope to describe the system in terms of a dynamical system having many fewer than roughly 1000 degrees of freedom that we have been allowing in our spectral simulations.

As in the case of the small scale structures, the average drift speed diminishes to zero for the chaotic regimes and the drift is not present at all for $\Omega \geqslant 12.5\Omega_c$.

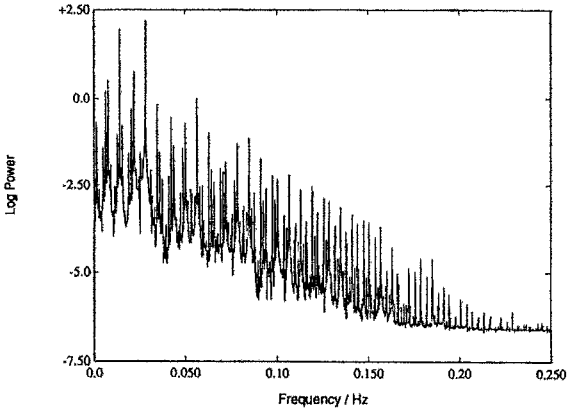

FIG. 21. Power spectrum of the velocity u at $\Omega = 10.7\Omega_c$. One period doubling has taken place in the range $9.65 \leqslant \Omega/\Omega_c \leqslant 10.7$.

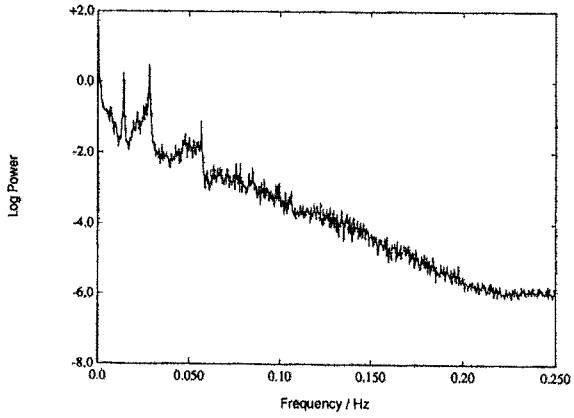

FIG. 22. Power spectrum of the velocity u at $\Omega = 10.805\Omega_c$. The flow is chaotic, but the principal frequency and its subharmonics are dominant in the spectrum.

This concludes our detailed description of the behavior of the fixed point (21) of the Kolmogorov flow as a function of the bifurcation parameter Ω.

VI. SUMMARY

In this paper we investigated in some detail a simple fluid governed by the incompressible two-dimensional Navier–Stokes equations with a spatially periodic time-independent forcing. Two main regimes of the flow have been observed: small and large scale structure regimes corresponding to different ranges of Reynolds number Re. A sequence of bifurcations takes place in each of the regimes of the flow.

The first three bifurcations taking place in the small scale structure regime are steady: the first corresponds to the appearance of the cellular structures, the second doubles the horizontal wave number of the cellular structures, while the third breaks the symmetry of the flow. In addition, three chaotic windows are discovered in the small scale structures regime. The first window is chaotic over a very long time scale. The second window is an intermittency with a remarkable feature that the chaotic flow has *nonunique* attractors. Finally, the last chaotic window shows intermittency with one connected chaotic attractor consisting of eight symmetric components ("butterflies"). There are laminar windows between the first and the second chaotic regimes, and after the last chaotic regime.

The large scale structure regime contains a number of periodic and chaotic windows. Before the formation of the large scale structures, the flow spends considerable time in *metastable* chaos that approaches true turbulent flow for the range of Re under the discussion. A spatially disordered, but temporally steady state was observed between the first two laminar windows. Two period doublings take place in the second laminar window. The chaotic regime that follows has the same remarkable property of chaotic but *nonunique* attractors as is the case with the small scale structure regime. In addition, there is a window of relaminarization with a

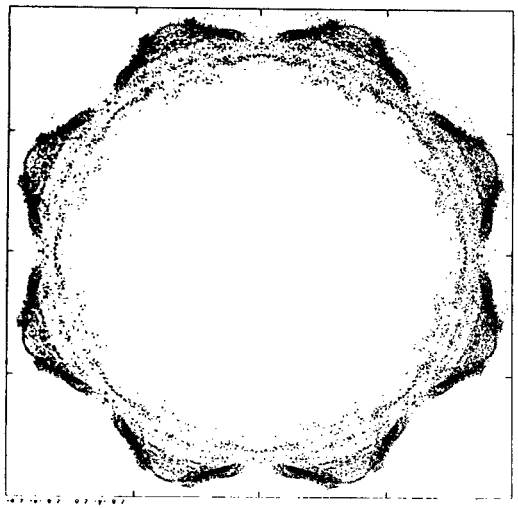

(a)

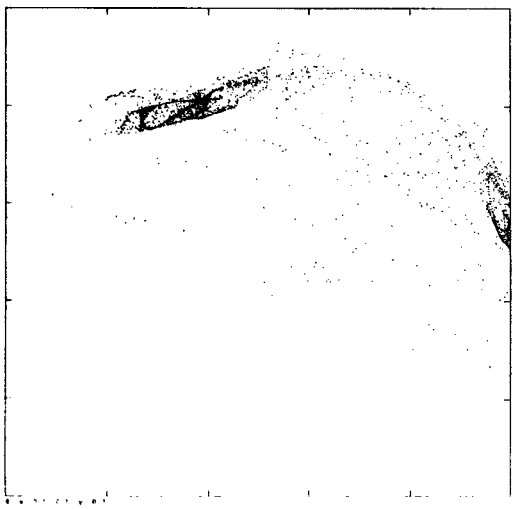

(b)

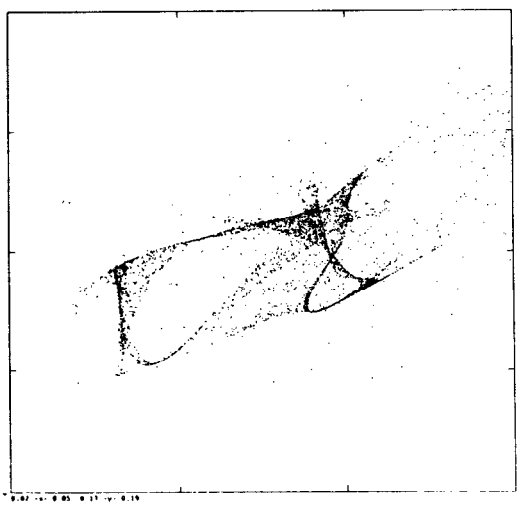

(c)

FIG. 23. (a) Poincaré section of the chaotic attractor at $\Omega = 10.805\Omega_c$; (b) and (c) are blowups of one of the components of the attractor. The fractal structure of the attractor is evident from blowups.

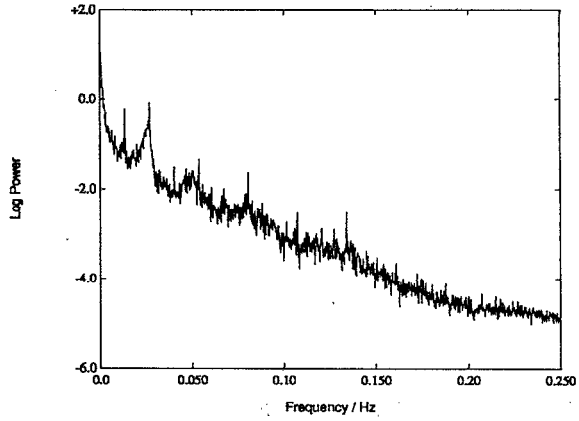

FIG. 24. Power spectrum of the velocity u at $\Omega = 12.5\Omega_c$. The principal frequency and its subharmonics are still dominant in the spectrum.

periodic flow between the two chaotic regimes.

In the future, we plan to use the proper-orthogonal decomposition[49] to extract the coherent structures of the flow and study the resulting low-order dynamical systems.[50]

ACKNOWLEDGMENTS

The work was supported by DARPA-URI Grant No. N00014-86-K0754. Numerical simulations were carried out on the NAS facility at the NASA–Ames Research Center and at the Pittsburgh Supercomputer Center. Research was supported in part by the National Aeronautics and Space Administration under Contract No. NAS1-18605 while L. Sirovich and N. Fitzmaurice were in residence at the Institute for Computer Applications and Science and Engineering, Hampton, Virginia.

[1] J. P. Gollub and S. V. Benson, J. Fluid Mech. **100**, 449 (1980).
[2] A. Brandstater, J. Swift, H. Swinney. H. L. Wolf, D. Farmer, E. Jen, and P. Crutchfield, Phys. Rev. Lett. **51**, 1442 (1983).
[3] P. R. Fenstermacher, H. L. Swinney, and J. P. Gollub, J. Fluid Mech. **94**, 103 (1979).
[4] B. Malraison, P. Atten, P. Berge, and M. Dubois, C. R. Acad. Sci. Paris C **297**, 209 (1983).
[5] L. Keefe, Stud. Appl. Math. **73**, 91 (1985).
[6] C. Doering, J. D. Gibbon, D. Holm, and B. Nicolaenko, *Low Dimension Behavior in the Complex Ginzburg-Landau Equation* (Contemporary Mathematics/American Mathematical Society, Providence, RI, 1989).
[7] L. Sirovich and J. D. Rodriguez, Phys. Lett. A **120**, 121 (1987).
[8] L. Sirovich, J. D. Rodriguez, and B. Knight, Physica D **43**, 63 (1990).
[9] A. C. Newell and J. A. Whitehead, J. Fluid Mech. **38**, 279 (1969).
[10] A. C. Newell, *Envelope Equations, in Nonlinear Wave Motion* (American Mathematical Society, Providence, RI, 1974).
[11] L. M. Hocking, K. Stewartson, and J. T. Stuart, J. Fluid Mech. **51**, 705 (1972).
[12] H. Hasimoto, and H. Ono, J. Phys. Soc. Jpn. **33**, 805 (1972).
[13] L. Sirovich and A. E. Deane, J. Fluid Mech. **222**, 251 (1990).
[14] V. I. Arnold and L. D. Meshalkin, Usp. Mat. Nauk **15**, 247 (1960).
[15] L. D. Meshalkin and Ia. G. Sinai, Prik. Mat. Mech. **25**, 1140 (1961).
[16] J. S. A. Green, J. Fluid Mech. **62**, 273 (1974).
[17] G. I. Sivashinsky, Physica D **17**, 243 (1985).
[18] R. H. Kraichnan, Phys. Fluids **10**, 1417 (1967).

[19] G. K. Batchelor, Phys. Fluids (Suppl. 2) **12**, 233 (1969).
[20] G. I. Sivashinsky and V. Yakhot, Phys. Fluids **28**, 1040 (1985).
[21] V. Yakhot and G. I. Sivashinsky, Phys. Rev. A **35**, 815 (1987).
[22] J. Kaplan and J. Yorke, in *Functional Differential Equations and Approximation of Fixed Points*, edited by H. O. Peitgen and H. O. Walther (Springer, New York, 1979).
[23] J. M. Ottino, C. W. Leong, H. Rising, and P. D. Swanson, Nature **33**, 419 (1988).
[24] H. Aref, J. Fluid Mech. **143**, 1 (1984).
[25] V. Rom-Kedar, A. Leonard, and S. Wiggins, J. Fluid Mech. **214**, 347 (1990).
[26] Z. S. She, in *Proceedings on Current Trends in Turbulent Research* (AIAA, New York, 1988), pp. 374–396.
[27] Z. S. She, Phys. Lett. A **124**, 161 (1987).
[28] Z. S. She and B. Nicolaenko, in *IUTAM Symposium*, August 1989 (Cambridge U. P., Cambridge, 1989).
[29] B. Nicolaenko and Z. S. She, in Proceedings of the Kiev Conference, Kiev, 1989.
[30] P. G. Drazin and W. H. Reid, *Hydrodynamic Stability* (Cambridge U. P., Cambridge, 1981).
[31] L. Sirovich, Q. Appl. Math. **45**, 573 (1987).
[32] G. Birkoff and S. MacLane, *Survey of Modern Algebra* (MacMillan, New York, 1941).
[33] C. Canuto, M. Y. Hussaini, A. Quarderonic, and T. A. Zang, *Spectral Methods in Fluid Dynamics* (Springer, New York, 1987).
[34] O. A. Ladyshenskaya, *The Mathematical Theory of Incompressible Viscous Flow* (Gordon and Breach, New York, 1969).
[35] A. Leonard and A. Wray, in *Proceedings of the 8th International Conference on Numerical Methods in Fluid Dynamics*, Aachen, Lecture notes in Physics, edited by E. Krause (Springer, New York, 1982), Vol. 170.
[36] P. Berge, Y. Pomeau, and C. Vidal, *Order Within Chaos* (Wiley, New York, 1986).
[37] G. L. Bennetin, L. Galgani, A. Giogilli, and J. Strelcyn, Meccanica **15**, 9 (1980).
[38] I. Shimada and T. Nagashima, Prog. Theor. Phys. **61**, 1605 (1979).
[39] A. Wolf, J. B. Swift, H. L. Swinney, and J. A. Vastano, Physica D **16**, 285 (1985).
[40] N. Fitzmaurice (MacGiolla Mhuiris), Adv. Comput. Methods P.D.E. **6**, 460 (1987).
[41] P. Constantin, C. Foiaş, O. P. Manley, and R. Temam, J. Fluid Mech. **150**, 427 (1985).
[42] N. F. Bondarenko, M. Z. Gak, and F. V. Dolzhansky, Atmos. Ocean. Phys. **15**, 711 (1979).
[43] D. Armbruster, J. Guckenheimer, and P. Holmes Physica D **29**, 257 (1988).
[44] N. Aubry, P. Holmes, J. L. Lumley, and E. Stone, J. Fluid Mech. **192**, 115 (1988).
[45] C. Grebogi, E. Ott, F. Romeiras, and J. A. Yorke, Phys. Rev. A **36**, 5365 (1987).
[46] C. Grebogi, E. Ott, and J. A. Yorke, Science **238**, 632 (1987).
[47] C. Basdevant, B. Legras, R. Sadourney, and M. Beland, J. Atmos. Sci. **30**, 2305 (1981).
[48] R. Benzi, G. Paladin, S. Patarnello, P. Santagelo, and A. Vulpianti, J. Phys. A Math. Gen. **19**, 3771 (1986).
[49] L. Sirovich, Q. Appl. Math. **45**, 561 (1987).
[50] L. Sirovich, Q. Appl. Math. **45**, 583 (1987).